JOURNAL OF NEUROPHYSIOLOGY
Vol. 71, No. 5, May 1994. *Printed in U.S.A.*

NASA-TM-111787

Compartmental Modeling of Rat Macular Primary Afferents From Three-Dimensional Reconstructions of Transmission Electron Micrographs of Serial Sections

THOMAS C. CHIMENTO, DAVID G. DOSHAY, AND MURIEL D. ROSS
NASA Ames Research Center, Life Sciences Biocomputation Center, Moffett Field, California 94035-1000

SUMMARY AND CONCLUSIONS

1. We cut serial sections through the medial part of the rat vestibular macula for transmission electron microscopic (TEM) examination, computer-assisted three-dimensional (3-D) reconstruction, and compartmental modeling. The ultrastructural research showed that many primary vestibular neurons have an unmyelinated segment, often branched, that extends between the heminode [putative site of the spike initiation zone (SIZ)] and the expanded terminal(s) (calyx, calyces). These segments, termed the neuron branches, and the calyces frequently have spinelike processes of various dimensions that morphologically are afferent, efferent, or reciprocal to other macular neural elements. The purpose of this research was to determine whether morphometric data obtained ultrastructurally were essential to compartmental models [i.e., they influenced action potential (AP) generation, latency, or amplitude] or whether afferent parts could be collapsed into more simple units without markedly affecting results. We used the compartmental modeling program NEURON for this research.

2. In the first set of simulations we studied the relative importance of small variations in process morphology on distant depolarization. A process was placed midway along an isolated piece of a passive neuron branch. The dimensions of the four processes corresponded to actual processes in the serial sections. A synapse, placed on the head of each process, was activated and depolarization was recorded at the end of the neuron branch. When we used 5 nS synaptic conductance, depolarization varied by 3 mV. In a systematic study over a representative range of stem dimensions, depolarization varied by 15.7 mV. Smaller conductances produced smaller effects. Increasing membrane resistivity from 5,000 to 50,000 Ωcm^2 had no significant effect.

3. In a second series of simulations, using whole primary afferents, we examined the combined effects of process location and afferent morphology on depolarization magnitude and latency, and the effect of activating synapses individually or simultaneously. Process location affects peak latency and voltage recorded at the heminode. A synapse on a calyceal process produced $\leq$8% more depolarization and a 23% increase in peak latency compared with a synapse on a process of a neuron branch. For whole primary afferents, depolarization decreased 40% between simulations of the smallest and largest afferents. Simulations in which membrane resistivity and synaptic conductance were varied while afferent geometry was kept constant indicated that use of 5,000 Ωcm^2 and 1.0 nS produced results that best fit electrophysiological findings. Synaptic inputs activated simultaneously did not sum linearly at the heminode. Total depolarization was ~14% less than a simple summation of responses of synapses activated one at a time.

4. In a third set of simulations we examined the effects of including an active SIZ on synapse summation and AP generation. Adding an active SIZ at the heminode decreased total depolarization and increased the rate of repolarization compared with the passive condition. Production of an AP at the SIZ depended on the number of synapses on the primary afferent, synaptic conductance, and membrane resistivity. Activating synapses beyond those required to reach AP threshold decreased AP peak latency by $\leq$54%.

5. In a fourth set of simulations we examined the effects of stem morphology and process location (calyx or neuron branch) on depolarization at the head of an efferent process when the depolarization source was located proximally. Under these conditions stem morphology had virtually no effect on the voltage or peak latency recorded at the head of efferent processes. Membrane resistivity also had no effect. The location of an efferent process on the primary afferent minimally affected depolarization magnitude and peak latency.

6. In the final simulations we examined effects of recurrent synapse activity when process heads were depolarized with local synaptic input. The morphology of the stem altered the magnitude of depolarization recorded at the head by >45 mV when 5 nS synaptic conductance was used. This range increased to 53 mV at 1 nS and was reduced to 24 mV at 0.1 nS.

7. Taken together, the results demonstrate that measurements available only from TEM are critical to compartmental models of neuronal functioning. Furthermore, by including known morphological details (for example, the number and location of synapses), reasonable estimates for model parameters can be made. TEM is required for accurate measurements of 3-D structures. Light microscopy does not provide adequate resolution for precise measurements or for determining synaptic distribution. The implications for understanding vestibular endorgan functioning are discussed.

INTRODUCTION

Mammalian vestibular maculae are sensory endorgans that are responsive to linear acceleration. Primary afferent endings in the maculae have a unique morphology (Fig. 1). Large terminal calyces wrap around the bodies of type I hair cells. Each calyx can contain from one to five type I hair cell(s) and as many as four calyces have been seen on a single primary afferent in the rat macula (Ross et al. 1990a,b). Synaptic input to the calyx from a type I hair cell occurs largely at the base of the hair cell. Type II hair cells, which synapse with the outer membrane of calyces and with the heads of afferent processes, provide additional input to the primary afferents.

There are three types of afferent terminal endings based

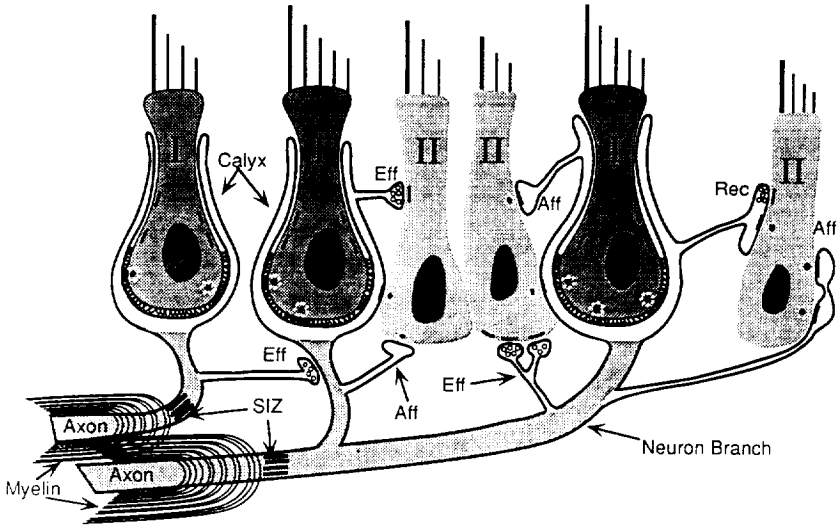

FIG. 1. Schematic representation of the principal innervation patterns of hair cells within the utricular macula of the rat. Type I and type II hair cells are the sensory receptor cells. The calyx wraps around the bodies of type I hair cells. An unmyelinated neuron branch begins at the base of each calyx (shaded areas). When there is >1 neuron branch, the branches connect distal to the 1st heminode. The heminode is the assumed site of the spike initiation zone (SIZ). Processes contribute to the afferent (Aff) input by receiving synaptic transmission from type II hair cells. Processes may provide efferent (Eff) output to type II hair cells or neuron branches through presynaptic contacts. The type II hair cell at *far right* displays a recurrent (Rec) synapse. There are presynaptic vesicles and a postsynaptic thickening together in a single process head. This diagram does not include all the possible connections found in the macula. For example, this diagram does not include efferent endings described as originating from the CNS.

on the position of the first heminode. In the M-type terminal the heminode is at the base of the calyx. In the M/U type there is a short (1.0–2.0 μm) unmyelinated segment before the heminode, referred to here as the neuron branch. In the U type the neuron branch varies in length from a few micrometers to $\geq$100 μm. U-type nerve fibers predominate in the macula, accounting for possibly $\geq$80% of the afferents in rat maculae. U-type primary afferent endings consist of six main components: *1*) one or more calyces, *2*) neuron branches, *3*) afferent processes, *4*) efferent processes, *5*) recurrent processes, and *6*) myelinated axons with a spike initiation zone (SIZ, i.e., 1st heminode) and nodes of Ranvier (Fig. 1). Only U-type fibers are simulated in this study.

Emanating from the neuron branch and calyx are projections called processes. The processes are similar in some ways to the spines found on pyramidal cell dendrites (Segev and Rall 1988; Wilson 1992). Like spines, vestibular afferent processes consist of a stem and a bulbous head. However, most processes are larger than dendritic spines and they lack a spine apparatus. Ultrastructural research and three-dimensional (3-D) reconstructions reveal a wide range of synaptic connections on macular receptor cells and primary afferents and a complex connectivity between the neural elements. Most processes are postsynaptic to ribbon synapses in the type II cells, i.e., the processes are afferent endings. Other processes contain numerous vesicles and on morphological grounds are efferent (Fig. 1). They make horizontal connections to adjacent type II hair cells where they end opposite subsynaptic cisterns (c synapses, Conradi 1969; McLaughlin 1972) or terminate as asymmetric synapses on calyces and other neuron branches. Finally, some processes contain both pre- and postsynaptic elements, defining them as recurrent (also known as reciprocal). Current physiological techniques are not capable of exploring the functions of processes. This makes compartmental modeling appealing as a method to investigate the effects of morphology on voltage spread within single primary vestibular afferents.

Compartmental modeling has been used to *1*) determine whether large dendritic trees can be collapsed into simpler equivalent cylinder representations (Durand et al. 1983; Jack and Redman 1971; Rall 1962, 1984; Rose and Vanner 1988), *2*) examine depolarization within single cells (Brown et al. 1981; Coleman and Miller 1989; Koch et al. 1992), *3*) confirm the quality of electrophysiological recordings (Hestrin et al. 1990), and *4*) study the connections between two or more cells (Shepherd and Brayton 1979). Although many of the original models explored passive flow of current in dendrites and dendritic spines (Rall 1967, 1969a,b; Rall and Shepherd 1968), later simulations included active channels (Segev and Rall 1988; Shepherd et al. 1985). The simulations of dendritic spines led us to use compartmental models to examine similar questions for analogous structures (processes) on primary afferents in the vestibular endorgan.

In this report we describe results of computer simulations based on compartmental models that address the following issues: *1*) the relative synaptic contribution to afferent output when stem dimension is varied, *2*) synaptic summation, *3*) the properties of efferent processes, and *4*) the properties of recurrent connections. A primary goal was to determine whether employing the accuracy of ultrastructural morphometry in compartmental models of neural electrodynamics affects action potential (AP) generation and peak latency (henceforth referred to simply as latency) or peak depolarization magnitude (henceforth referred to as depolarization magnitude or depolarization) at the heads of efferent and recurrent processes. We used data from serial sections and from 3-D reconstructions to build our neuron models and we examined the consequences of varying membrane resistivity and synaptic conductance. We started with compartmental models of definable pieces of a neuron, added new parts, and finally constructed a vestibular neuron terminal for analysis. Our results show that variations in morphology determined from serial section electron microscopy can affect the outcome of compartmental model simulations. The findings demonstrate that there is a range of simulation parameters that best match experimental results.

Preliminary results of this work have been presented at the Society for Neuroscience meeting (1991), the Analysis and Modeling of Neural Systems meeting (1991), and the Computational Neural Systems meeting (1992).

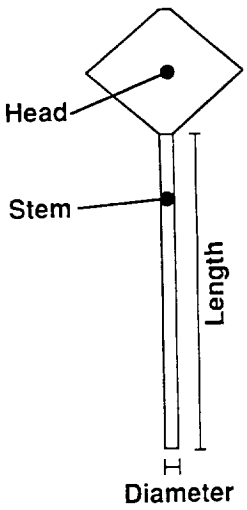

FIG. 2. Diagram of the processes attached to a neuron branch showing the terms used to describe the main parts and their measurements. This process shape is representative of commonly observed processes.

METHODS

Histology

Rat utricular maculae were fixed by perfusion with 2.5% glutaraldehyde and 0.5% paraformaldehyde in 0.1 M Millonig phosphate buffer, pH 7.4. All tissues were postfixed for 1 h in 1.0% osmium tetroxide in Millonig phosphate buffer and dehydrated in steps from 30% to 70% ethanol. Samples were then microdissected to obtain maculae free of temporal bone, dehydration was completed, and the tissues were embedded in Spurr resin. After sectioning at 1 μm to reach the area of choice, ultrathin sections ($\sim$0.15 μm) were cut on a Reichart ultramicrotome. Sections were mounted on slot grids previously coated with Formvar, then stained with 4% uranyl acetate and 2% lead citrate.

Electron microscopy and reconstructions

Electron micrograph mosaics of serial sections were used to produce 3-D images of vestibular primary afferent endings. Each reconstruction was made using 300–600 serial sections. Every third or fifth section was photographed at ×3,000 magnification and micrographs were printed at ×4,500 magnification for the mosaics. Selected afferent terminals and all hair cells contacting them were traced onto acetate sheets. The tracings were digitized into a PC and reassembled as filled slice reconstructions (Kinnamon et al. 1986; Young et al. 1987). Data were transferred to a Silicon Graphics IRIS 4D/210 VGX graphics workstation for 3-D reconstruction using software developed in our laboratory.

Simulations

The compartmental modeling program NEURON (Hines 1989, 1991), which uses one-dimensional (1-D) cable "sections" to analyze voltage changes, was used for the simulations. Each section is composed of a user-specified number of cylindrical isopotential compartments. The sections can be connected to construct an arbitrary branched cable. Membrane properties, such as resistivity, capacitance, reversal potential, and the presence of Hodgkin-Huxley membrane mechanisms, can be specified for any section.

Measurements of the diameter and length of processes obtained from electron micrographs were used to construct schematic representations for analysis (Fig. 2). The measurements were taken where the taper rate of the process changed. This resulted in a process composed of sections, each section being a cylinder or frustrum. Frustrums were approximated by a series of stacked cylindrical isopotential compartments varying linearly in diameter.

The number of compartments used in a simulation was derived empirically by increasing compartments until a finer spatial mesh did not markedly affect the results of the computation. Thus all process sections were modeled using 30 compartments and the neuron branch was modeled with 100 compartments. When an entire afferent ending was simulated each neuron branch and each calyx were modeled with 10 compartments. Axons were constructed with 10-compartment internodal regions and a 1-compartment node of Ranvier. Using 692 compartments for a simulation of an entire afferent and a time step of $1/500\ \tau$ (the time constant of the membrane) a single simulation took <1 min to run on a Sun SPARC station 4/370.

All the local electrical properties used here, such as cytoplasmic resistivity and the widely accepted value of 1 μF/cm^2 for specific membrane capacitance, are taken from the literature (Brown et al. 1981; Cherubini et al. 1988; Durand et al. 1983; Hestrin et al. 1990; Johnston and Brown 1983; Rajan and Jahnstone 1988; Randall et al. 1990; Rose and Vanner 1988; Segev and Rall 1988; Yamaguchi and Ohmori 1990). For all simulations the axial (cytoplasmic) resistivity was 100 Ωcm and resting membrane potential was set at -65 mV. Simulations were run with membrane resistivity of 5,000, 20,000, or 50,000 Ωcm^2. The calyces, processes, and neuron branches were all modeled as passive structures. To simulate the SIZ and nodes of Ranvier we multiplied the maximum sodium, potassium, and leakage conductances in the Hodgkin-Huxley equations by 100 and adjusted the rate function to 15°C. These parameters produced simulated APs that approximated the duration and amplitude of mammalian responses. To model the insulating property of the myelinated axon we increased the specific membrane resistivity along internodal regions to 1 MΩcm^2.

A synapse, modeled as a time-varying conductance, was located on the distal end of each process or near the base of a calyx. The time course of the conductance for all simulations was modeled as a standard α-function, with a time to peak of 0.25 ms, a maximum synaptic conductance (g_{syn}) of 0.1, 1, or 5 nS, and an absolute reversal potential of 0 mV.

Simulated voltage was recorded at three sites on the isolated neuron branch: *1*) at one end of the neuron branch, *2*) at the distal end of efferent processes (a presynaptic site in the head), and *3*) at the distal end of the process containing a recurrent synapse (the head; see Fig. 2). In simulations of an entire primary afferent, measurements at the SIZ replaced recordings at the end of the neuron branch.

Calyx model

Calyx endings pose a unique problem for compartmental modeling. Their structure can be described as a two-membrane, planar surface wrapped around the type I hair cell(s). Numerical methods for two-dimensional current spread (Jack et al. 1983), needed to model the calyx properly, are under development. Here the calyx is modeled as a 1-D cable on the basis of the need to use conventional methods of compartmental modeling before implementing new procedures for two dimensions and on our desire to compare results of the two methods, which differ enormously in their computational loads.

The morphology of the calyx is difficult to convert to a form that can be analyzed with 1-D cable equations. Our solution was to approximate the calyx as a cylinder within a cylinder, each cylinder representing one cell membrane. The lengths of the cylinders were measured from each reconstructed calyx. The area of the annulus produced by the two cylinders was used to define a single

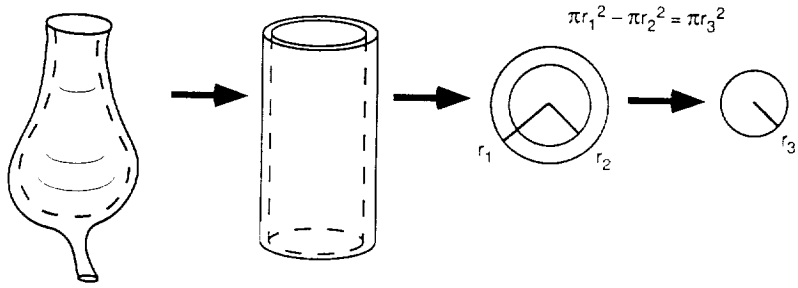

FIG. 3. Procedure for converting a calyx into an equivalent cylinder for entry into NEURON. First the calyx is approximated by a cylindrical annulus. The radius of the inner membrane (r_2) and that of the outer membrane (r_1) are determined from measurements of three-dimensional (3-D) reconstructions of calyces. The "cylinder within a cylinder" provides a close approximation of the total surface area and volume measured from the original calyx. The 2 radii are used to produce a single cylinder with a cross-sectional area equivalent to the annulus. The radius of this equivalent cylinder (r_3) is entered into the model along with the measured length of the original calyx. The membrane capacitance (C_m) of the calyx is increased to 2 $\mu F/cm^2$ and the membrane resistivity (R_m) decreased to 2,500 Ωcm^2 to compensate for the near-halving of the total membrane surface area.

cylinder of equivalent cross-sectional area for use in the simulations (Fig. 3). The reasoning was that this produced a good set of approximations for the length of the calyx, the volume of cytoplasm, and the cross-sectional area of the calyx. Therefore the resistance to current flow along the length of the equivalent cylinder calyx approximated the resistance of the calyx.

The one parameter of the equivalent cylinder approximation of the calyx that was not accurate was the total surface area, which was less than that of the original calyces largely because the calyx has inner and outer membranes. To account for this discrepancy we increased the specific membrane capacitance to 2 $\mu F/cm^2$ and decreased the membrane resistivity to 2,500 Ωcm^2. These changes in the calyceal membrane made the total capacitance, resistance, and time constant of the equivalent cylinder representation of the calyx closely approximate the values in the original calyx.

RESULTS

Simulations of a process on a neuron branch

EFFECT OF PROCESS MORPHOLOGY ON DEPOLARIZATION MAGNITUDE AND LATENCY. In the first set of four simulations we used an isolated neuron branch 112 μm long and 2.5 μm diam, with morphologically different processes (Fig. 4) emanating from the center. Process dimensions were obtained from serial section micrographs. Voltage was recorded at one end of the neuron branch.

As seen in Fig. 4, maximum depolarization at the end of the neuron branch may vary slightly for different process geometries. However, the traces in Fig. 4, *C* and *D*, are identical. The peak amplitude of depolarization at the end of the neuron branch is less in *C* and *D* than in *A* and *B*. However, the latency is similar for all four processes. Whether the variation in amplitude and latency measured in the simulations has functional significance, such as altering the requirements for AP generation, will be addressed later in this report.

EFFECTS OF STEM DIMENSION ON VOLTAGE. The above simulations provided an indication that morphological details of a process influence the magnitude of depolarization recorded at a distant site. However, the dimensions of the processes used in the above simulations did not cover the full range of stem lengths and diameters observed in the rat utricular macula. Therefore we systematically examined the effects of length and diameter (see Fig. 2 for definitions) by varying the diameter of the stem while keeping all other parameters constant and then by varying just the length of the stem while holding the diameter constant. Using this methodology we investigated a 6 × 6 matrix of possible stem sizes (Fig. 5). The lengths and diameters of the processes examined extended slightly beyond those measured in our sample of serial section electron micrographs because of the relatively small number of the longer and thinner processes that have been accurately measured. Two membrane parameters were varied: membrane resistivity and peak synaptic conductance. Selection these two parameters is difficult because of the range of values that have been measured experimentally. Membrane resistivity was set at 5,000, 20,000 and 50,000 Ωcm^2 and synaptic conductance at 5, 1, and 0.1 nS. All permutations of these parameters were tested. For the following simulations voltages were recorded at the end of the neuron branch.

Three sets of simulations are shown (Fig. 5, *A–F*). The *top row* displays the magnitude of depolarization from rest (−65 mV) and the *bottom row* is the latency. Membrane resistivity was 5,000 Ωcm^2 for all cases. Synaptic conductance was 5 nS for *A* and *B*, 1 nS for *C* and *D*, and 0.1 nS for *E* and *F*. The smaller dark region in Fig. 5*C* is the overlap between the stem dimensions of spines in the cerebellum (Harris and Stevens 1989) and vestibular afferent processes. The larger lined region is the overlap between stem dimensions of hippocampal CA1 spines (Harris and Stevens 1989) and vestibular afferent processes. The spine dimensions also extended off the matrix, because some spines are both thinner and shorter than any of the stems observed in the macula.

The results demonstrate that there can be a large range in magnitude of depolarization at the end of the neuron branch when the length and diameter of the stem are varied (Fig. 5*A*). The range of voltage values across the matrix in *A* is 15.7 mV (from 16.8 to 1.1 mV). Voltage increases are mostly restricted to the longest processes (16 μm) and occur when the diameter increases from 0.05 to 0.4 μm. When synaptic conductance is 1 nS the voltage range is reduced to 3.1 mV. Therefore there can be a sizable difference in depolarization across the range of stem dimensions commonly found in the utricular macula. This suggests that the contribution of a particular synapse to the total depolarization of

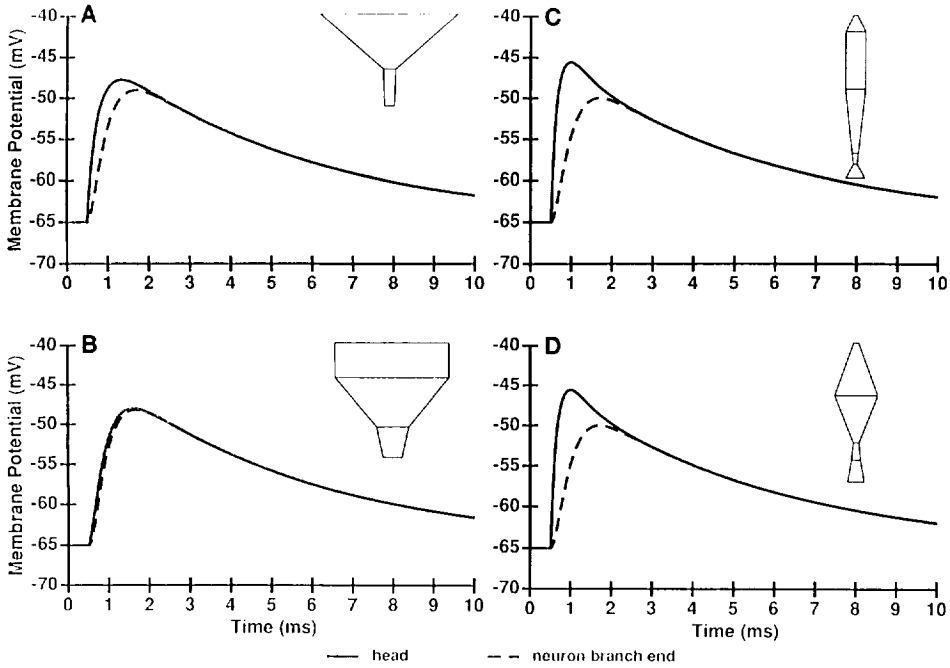

FIG. 4. Magnitude of depolarization for 4 different processes. The dimensions of these processes were measured from serial section electron micrographs. Depolarization was produced by placing a synapse, described by an α function [$g_{syn}e\alpha te^{-\alpha t}$ maximum synaptic conductance (g_{syn}) = 5 nS, time to peak (t_p) = α^{-1} = 0.25 ms], at the head. Recordings were made at the head (——) and at one end of the neuron branch (– – –). All membrane was passive. Axial (cytoplasmic) resistivity (R_i) = 100 Ωcm, C_m = 1 μF/cm^2. Synapse activation began at 0.5 ms.

a vestibular afferent needs to be specified in models of macular function.

When membrane resistivity was varied (not shown), virtually no change in the range of depolarization was observed with any of the three synaptic conductances tested.

EFFECTS OF STEM DIMENSION ON LATENCY. A gradual increase in latency occurred as stem diameter was varied from short and wide to long and thin. In general, increasing stem length increases latency and, conversely, increasing stem diameter decreases latency (Fig. 5*B*). Latency varied from 1.66 to 2.68 ms. This 1-ms range is sufficient to modify the temporal summation of simultaneous synaptic input.

Simulations of primary afferents with passive SIZ

EFFECTS OF PROCESS LOCATION ON VOLTAGE AND LATENCY MEASURED AT THE SIZ. Once we understood the effects of process morphology on depolarization using an isolated neuron branch, we expanded the simulations by using morphology from actual primary afferent endings. The first question posed was whether the location of a process affects depolarization magnitude and latency measured at the heminode (site of the SIZ). We selected four afferents for simulation (Fig. 6). Their dimensions were measured from 3-D reconstructions. Two identical processes were placed on each primary afferent, one on the calyx most distal to the SIZ (Fig. 6, arrows) and one on the neuron branch nearest the SIZ (Fig. 6, arrowheads). Membrane resistivity was set at 5,000 Ωcm^2 and synaptic conductance at 5 nS for the results shown in Fig. 7. We simulated synaptic input to the two processes separately and recorded the change in cell potential at the SIZ, i.e., at the first heminode of the afferent.

The results show that the magnitude of depolarization of an afferent decreases between 7.4 and 1.6% when the process is placed on the calyx rather than on the neuron branch (Fig. 7). This decrement is a result of leakage of current through the membrane that lies between the synaptic site on the calyceal process and the recording site on the nerve fiber branch. Along with the proximal flow of current, the calyx also provides a low resistance path for local synaptic currents to flow distally and a large surface area of membrane for current to leak through. Depolarization differs by ≤40% between the afferents simulated (compare Fig. 7, *A* and *D*). This is a consequence of the overall increase in surface area of the membrane, which permits more current to leak through the larger membrane surface area of the afferent (compare Fig. 6, *A* and *D*).

Latency increases 22% (0.33 ms) in the largest two afferents (Figs. 6, *B* and *D*, and 7, *B* and *D*) when the process is placed on the calyx rather than on the neuron branch. This increase is caused by the greater distance the current must travel to reach the SIZ and the additional time it takes to charge the membrane capacitance.

How would the choice of membrane resistivity and synaptic conductance affect these results? Simulations were conducted using the afferent from Fig. 6*A*. In Fig. 8 the synaptic conductance was held at 5 nS while the membrane resistivity was varied. Under these conditions depolarization varies by <1 mV. However, increasing the membrane resistivity also increases the time constant of the membrane and therefore the membrane remains depolarized longer.

Next the membrane resistivity was held constant at 50,000 Ωcm^2 while the synaptic conductance was varied from 5 to 0.1 nS. Under these conditions a large drop in depolarization of the membrane occurred (Fig. 9). The magnitude of depolarization declined nearly 75% between 5 and 1 nS. At 0.1 nS the cells were barely depolarized. However, the difference in excitatory postsynaptic potential (EPSP) magnitude remained proportional across the four afferents as the synaptic conductance was decreased.

From the previous results it appeared that stem morphology could significantly affect the depolarization at a proximal site along the afferent. Also, synaptic conductance affects the size of the EPSP, whereas membrane resistivity

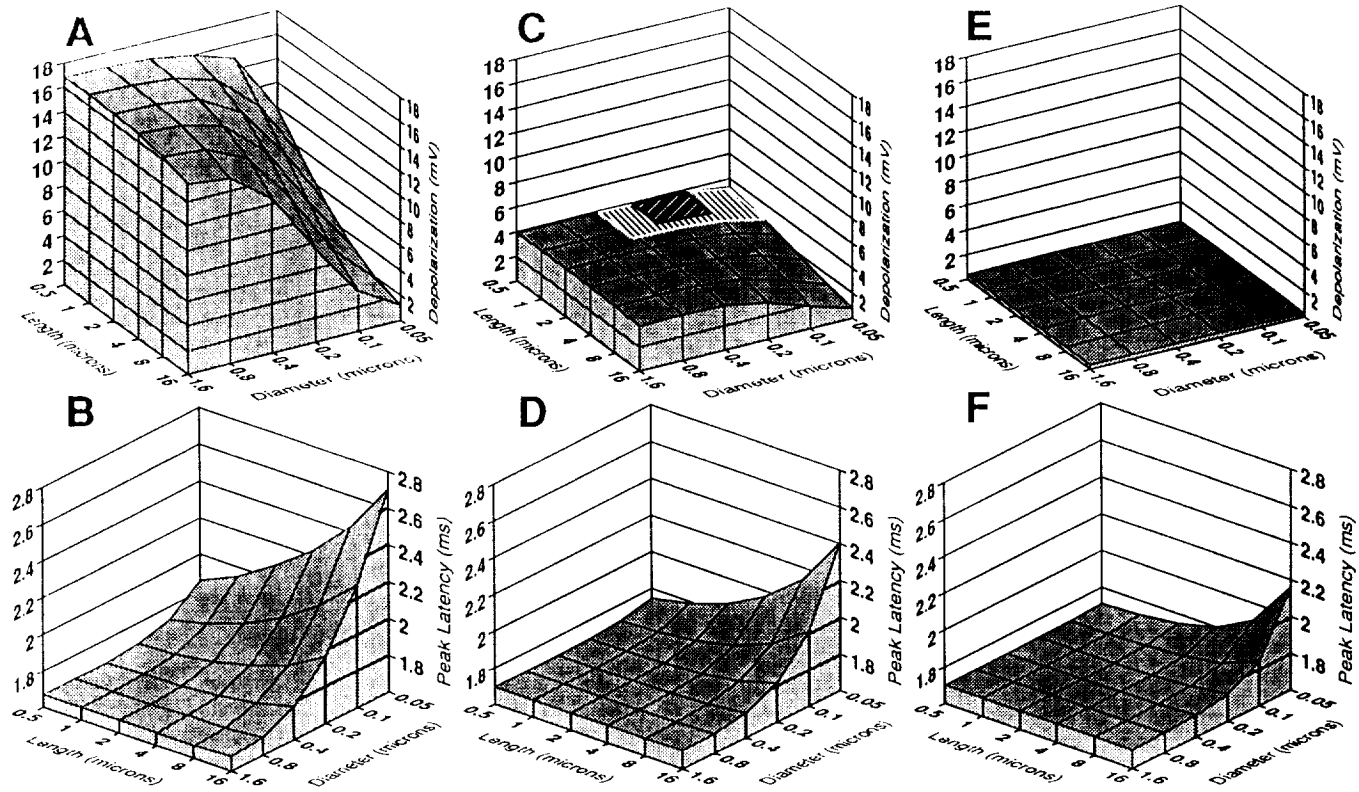

FIG. 5. Matrix of depolarization magnitude and latency as a function of stem length and diameter, and synaptic conductance. The lengths and diameters span the anatomically realistic ranges for stems; R_m = 5,000 Ωcm^2. *A* and *B*: synapse was located on the head of a process emanating from the center of a 112-μm-long neuron branch; g_{syn} = 5 nS. Recordings were made at one end of the neuron branch. Large variations in voltage [15.7-mV decrease (93%)] and latency [1.0-ms increase (38%)] occur between the shortest, thickest and the longest, thinnest stems. *C* and *D*: g_{syn} was reduced to 1 nS. Depolarization varies less as a function of morphology in this simulation than in *A* and *B*. However, the 3.1-mV difference between the shortest, thickest and the longest, thinnest stems is an 80% reduction in depolarization magnitude. *D*: latency showed a corresponding increase of 0.7 ms (42%). The smaller dark region in *C* is the overlap with the stem dimensions of spines in the cerebellum and the larger lined region is the overlap with hippocampal CA1 spines (Harris and Stevens 1989). *E* and *F*: g_{syn} was further reduced to 0.1 nS. There is virtually no variation in depolarization as stem morphology is changed. Latency increases slightly.

primarily affects the rate of return to the resting membrane potential. How could these results guide the selection of parameters for a whole-cell simulation? Would particular values be critical, or could the values vary with little effect on the result? To explore these questions we selected one primary afferent (Fig. 6*D*) and placed a total of four afferent processes on its calyces and neuron branches. One synapse was placed on each afferent process head and 10 synapses were placed near the base of each calyx. The total of 44 synapses and their distribution are representative of the population observed in mammalian endorgans. We used this afferent (Fig. 10) for a number of simulations described below.

SUMMATION OF SYNAPTIC INPUTS. In our previous simulations we examined the effects of process location on depolarization magnitude at the SIZ. In those simulations identical processes with identical synapses were placed at various locations on the afferent terminal. However, synapses along the inner membrane of the calyx from type I hair cells and along the outer membrane from the type II hair cells are more numerous sources of synaptic input to the afferent. Synapses on calyces were assessed by the next set of simulations using the representative afferent described above. In one case, active membrane was placed at the SIZ and at the nodes of Ranvier. Internodal regions were modeled as high-resistance regions of membrane (1 MΩcm^2).

For the simulation shown in Fig. 11, membrane resistivity was 5,000 Ωcm^2 and synaptic conductance was 1 nS. In the first simulation (solid line) the 44 synapses were activated 1 at a time and the individual results summed. In the second simulation (dashed line) all 44 synapses were activated simultaneously. In this case peak depolarization was ~14% less than the sum of the individual synaptic responses, demonstrating that synaptic currents did not sum linearly.

Simulations of primary afferents with active SIZ

Figure 11 (dotted line) illustrates the results of adding active membrane to the first heminode (the SIZ) and to nodes along the axon. Synapses were activated individually and their responses summed. In this case peak depolarization is reduced and the rate of repolarization is more rapid. An afterhyperpolarization similar to that observed after an AP is displayed, even though depolarization is subthreshold. These results demonstrate that simulation of subthreshold depolarizations on an afferent with only pas-

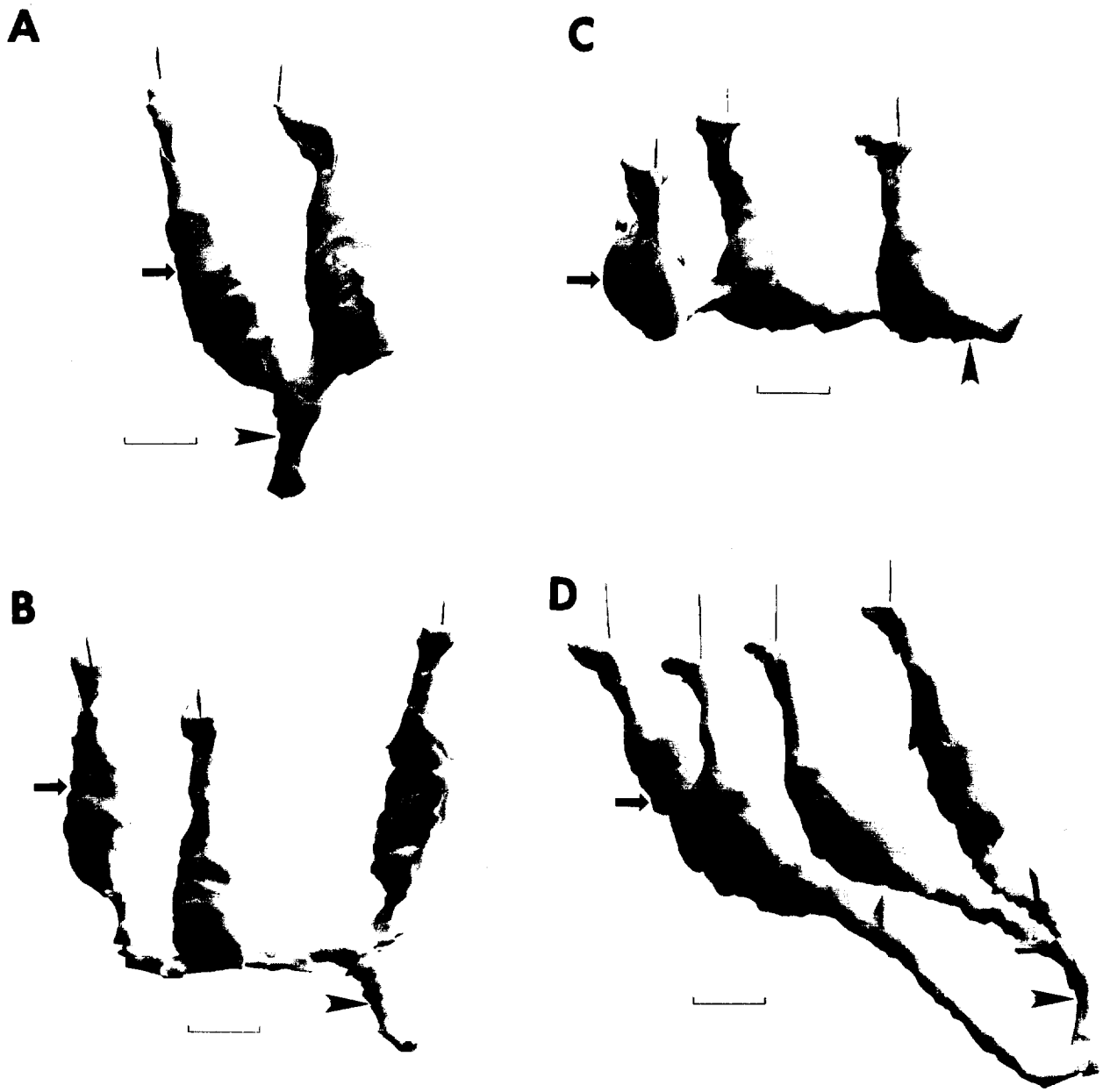

FIG. 6. 3-D reconstructions of 4 representative primary afferents. Arrow on each reconstruction: location of a process added to the model of a calyx. Arrowheads: location of a process added to the model of a neuron branch. These processes were not part of the original reconstructions but were placed at commonly observed sites to study systematically the effects of process location on depolarization magnitude at the SIZ. Scale bar: 10 μm.

sive properties yields different values from simulations that include active membrane at the SIZ.

Groups of synapses were activated simultaneously to determine whether the behavior of the AP is sensitive to changes in synapse number or membrane resistivity (Fig. 12). The thin solid line (*right*) shows that 20 is the minimum number of calyceal synapses required to reach AP threshold at 1 nS and 50,000 Ωcm^2. At 5,000 Ωcm^2 (dashed line) 23 synapses are required. Activating more synapses than required to reach threshold reduces the latency of the AP. The latency of the AP is reduced by >2.5 ms when the number of synapses is increased from 23 to 40 at 5,000 Ωcm^2 (thick solid line). At 50,000 Ωcm^2 (thick dashed line) latency is reduced by ~2 ms when the number of synapses is increased from 20 to 40. However, with 40 synapses (thick traces) the responses are virtually identical in both amplitude and latency. It is only near threshold that membrane resistivity affects AP latency or amplitude.

Simulation of efferent processes

EFFECTS OF STEM MORPHOLOGY ON VOLTAGE AND LATENCY AT THE DISTAL END OF AN EFFERENT PROCESS. Many of the processes on a primary afferent make presynaptic connections

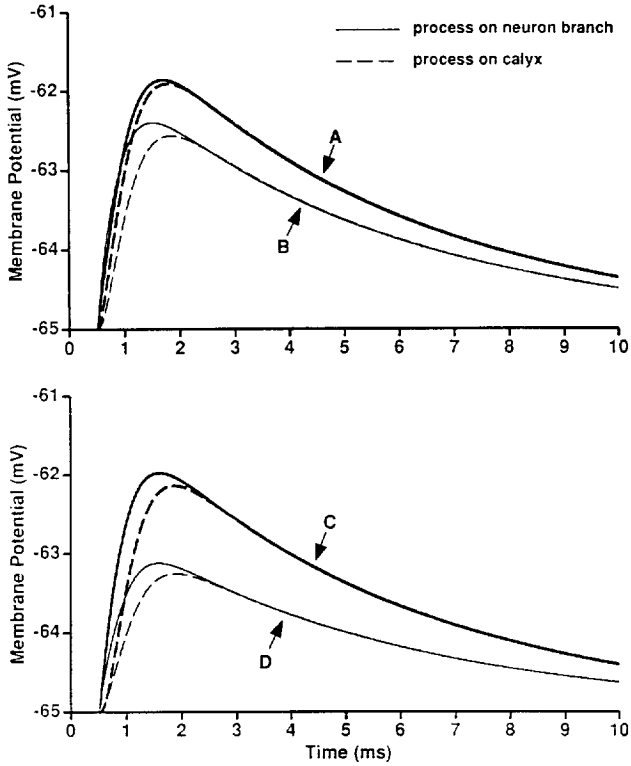

FIG. 7. Effects of process location within and across 4 different primary afferents. *A–D*: simulation results using dimensions measured from 3-D reconstructions of the primary afferents in Fig. 6, *A–D*. Dashed curves: depolarizations produced by processes on the calyx. Solid curves: processes on the neuron branch. Recordings were made at the heminode, which had no active channels (Hodgkin-Huxley-like). Variation in voltage between afferents in *A* and *D*, which have very different morphologies, is nearly 1.5 mV (a 40% decrease). Within any single afferent, process location has little effect on voltage. R_i = 100 Ωcm, R_m = 5,000 Ωcm², C_m = 1 μF/cm² for the neuron branches and processes and R_m = 2,500 Ωcm², C_m = 2 μF/cm² for the calyces (as described in legend of Fig. 3). Synapse activation began at 0.5 ms.

with adjacent type II hair cells, calyces, and neuron branches. These processes are arranged in a manner that would permit them to function analogously to interneur-

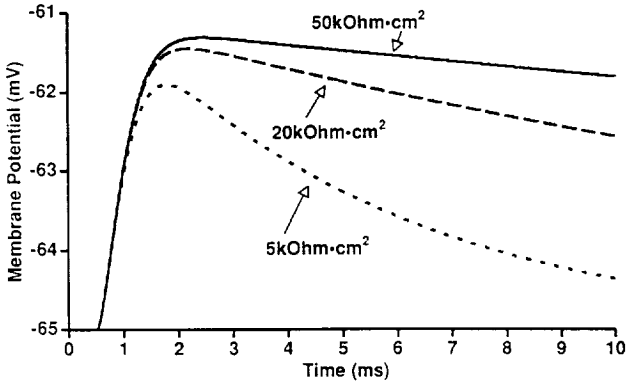

FIG. 8. Effects on excitatory postsynaptic potential (EPSP) magnitude when R_m is changed from 50,000 Ωcm² to 5,000 Ωcm² while g_{syn} is kept constant at 5 nS. Simulations were conducted using afferent from Fig. 6*A*. Depolarization is reduced by slightly more than 0.5 mV. However, the greatest effect is on the decay rate of the membrane potential. This is a consequence of decreasing the time constant of the membrane, thereby allowing the membrane to discharge more quickly.

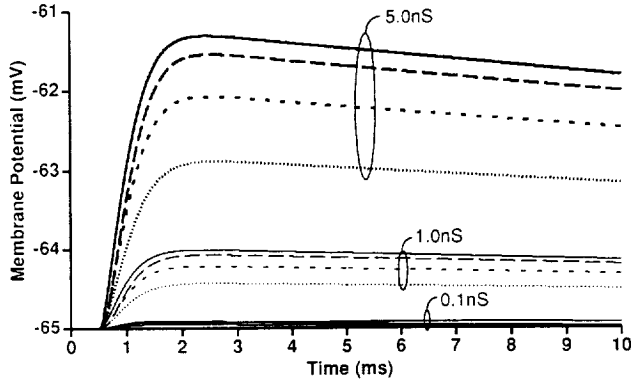

FIG. 9. EPSP magnitude as g_{syn} is varied from 5 to 0.1 nS. Simulations were conducted using afferent from Fig. 6*A*. R_m was set at 50,000 Ωcm² to prevent traces from overlapping. The EPSP magnitude remains proportional across the 4 afferents as synaptic conductance is decreased.

ons, but with only one synaptic delay. Just as local interneurons provide for communication within their territory, so would efferent processes communicate calyx or neuron branch activity to nearby type II hair cells, calyces, and neuron branches. This output could affect type II hair cell

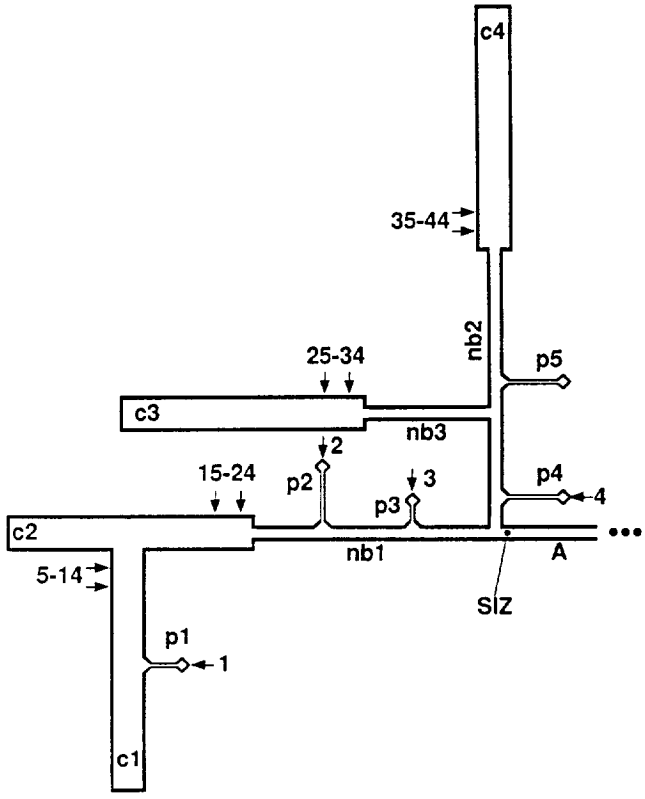

FIG. 10. Schematic of the reconstructed afferent in Fig. 6*D*. This diagram illustrates the general structure used in the simulation. A, axon; SIZ, heminode; nb1–nb3, 3 neuron branches; c1–c4, 4 equivalent cylinder calyces; p1–p5, 5 processes. The small numbered arrows on the calyces and process heads are the 44 synaptic inputs to the afferent, 10 on each calyx and 1 on each process. In all simulations calyces and neuron branches are divided into 10 compartments and processes are divided into 4 sections of 30 compartments each. The axon is composed of a 1-compartment heminode connected to a 30-μm, 10-compartment internode, followed by a 3-μm, 1-compartment node, a 1,000-μm, 10-compartment internode, and a final 3-μm, 1-compartment node. Nodes have active (Hodgkin-Huxley-like) membranes.

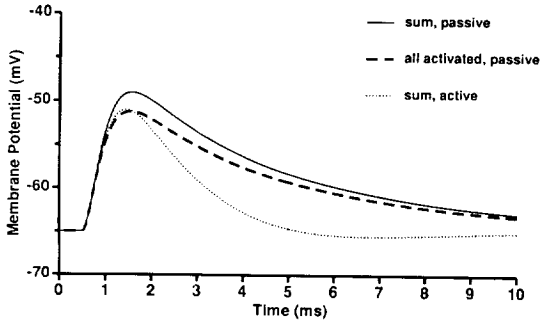

FIG. 11. Comparison between summation of all synapses activated individually and all synapses activated simultaneously. This simulation used the afferent shown in Fig. 10. R_m = 5,000 Ωcm^2, g_{syn} = 1 nS. The solid line is produced by the sum of 44 synapses activated individually on a passive afferent ending, and the heavy dashed line by the simultaneous activation of the same 44 synapses. The difference between these 2 traces demonstrates that summation of simultaneously activated synapses is nonlinear. The dotted line is the sum of 44 individually activated synaptic inputs with active nodes on the axon. Addition of Hodgkin-Huxley active sites to the nodes produces an intermediate amplitude response that repolarizes more quickly than either of the previous responses. Also, there is a clear afterhyperpolarization not seen in the other 2 traces.

activity, which would influence the output of vestibular afferents. Therefore for network modeling it is necessary to determine those factors that affect the magnitude of depolarization reaching presynaptic release sites in efferent processes.

A single 5-nS synapse on the neuron branch was activated to provide the current source. Depolarization magnitude (Fig. 13*A*) and latency (Fig. 13*B*) at the presynaptic site (head) of an efferent process are virtually unaffected by process morphology. There is a maximum increase of 0.43 ms and 0.2 mV between the shortest, large-diameter stem (0.5 × 1.6 μm) and the longest, thinnest stem (16 × 0.05 μm). Varying the membrane resistivity and synaptic conductance, as was done in previous simulations, simply shifted the matrix results up or down (not shown).

EFFECTS OF PROCESS LOCATION ON VOLTAGE AND LATENCY AT THE DISTAL END OF AN EFFERENT PROCESS. For the next simulation we placed four efferent processes at different locations on the representative afferent. All 44 synapses on the afferent were activated simultaneously, producing an AP at the SIZ. The AP was used as the source of current for depolarizing the cell and voltage was recorded at the terminal ends of the efferent processes. The distal voltage spread from the SIZ is nearly uniform at the distal end of an efferent placed at any site on the primary afferent (Fig. 14).

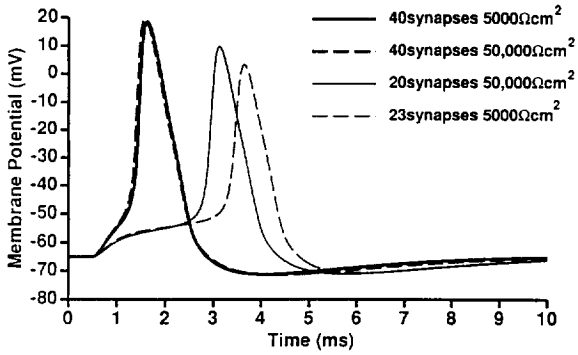

FIG. 12. Action potential (AP) as a function of synapse number and membrane resistivity. The 2 bold lines show the result of simultaneously activating 40 synapses. g_{syn} = 1 nS, R_m = 50,000 and 5,000 Ωcm^2. The difference between the thick solid and thick dashed lines is negligible. The 2 thin lines show the minimum number of synapses necessary to reach AP threshold when resistivity is varied. Reducing membrane resistivity increased the total number of synapses required for AP generation and also increased latency.

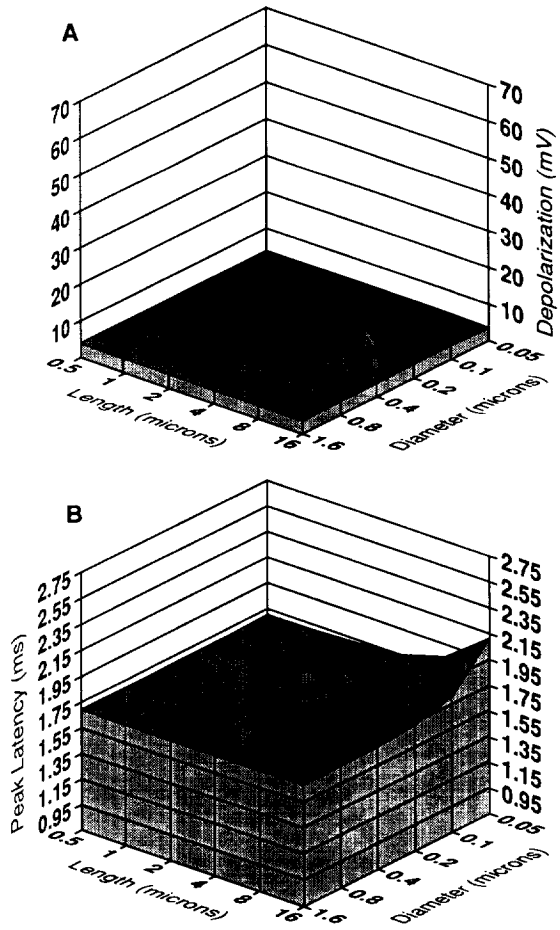

FIG. 13. Matrix of depolarization magnitude and latency at an efferent process head as a function of stem length and diameter. *A* and *B*: synapse was activated at a proximal site on the primary afferent and recordings were made at the head. All other parameters are the same as in Fig. 5*B*. With a proximal depolarization source, voltage and latency vary little at the distal end of an efferent process for the range of stem dimensions tested. When membrane resistivity and synaptic conductance were varied, the only change observed is a slight shift of the entire surface along the Z axis (not shown).

Simulations of recurrent connections

EFFECTS OF STEM MORPHOLOGY ON VOLTAGE. In many instances a postsynaptic site is located next to a presynaptic site within a process head (Fig. 1), forming a recurrent connection. In such a connection the postsynaptic depolarization produced in the process head may be sufficient to cause release of neurotransmitter to the type II hair cell. Therefore we simulated such a situation by recording the depolarization within a process head next to a synapse (Fig. 15). The membrane resistivity was kept constant at 5,000 Ωcm^2. The shaded regions in Fig. 15*C* are the overlaps between the

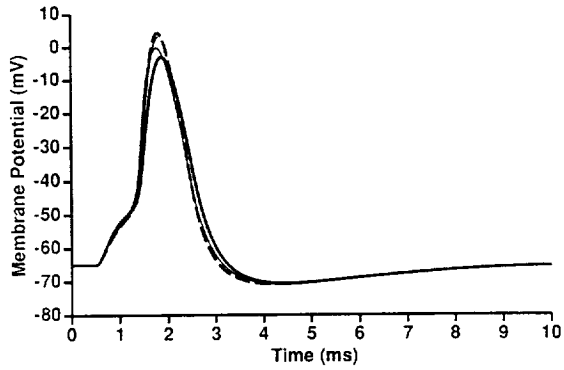

FIG. 14. Effect of location on efferent process depolarization. Processes were placed at 4 locations on the model neuron (Fig. 10). All 40 synapses on calyces were activated simultaneously. The depolarization reaching the efferent head after an AP fires (i.e., the distal spread of the AP) is minimally affected by process location. The depolarization varies from about −5 to +3 mV at the proximal end of c1 and the middle of nb1 (see Fig. 10), respectively.

stem dimensions of dendritic spines and vestibular afferent processes (see Fig. 5*C*).

In Fig. 15*A*, large variations in voltage [46.2-mV increase (270%)] between the shortest, thickest process and the longest, thinnest process are produced in the simulations. After reducing the synaptic conductance to 1 nS (Fig. 15*C*), depolarization varies more than in *A* [53.4-mV increase (1,340%)] because of saturation effects in *A*. The g_{syn} was further reduced to 0.1 nS in Fig. 15*E*. The variation in depolarization is 24.2 mV and the percentage is 5,865%. This large percentage is due to the extremely small depolarization with the shortest, thickest process stems (0.4 mV).

EFFECTS OF STEM MORPHOLOGY ON LATENCY. As shown in Fig. 15*B* (5 nS) variations in latency are moderate [0.8-ms decrease (47%)] when stem diameter and length are simultaneously varied. There is a steep decline in the middle region of the matrix. Across this middle region, very small changes in morphology can produce nearly the maximum change in latency. These changes are sufficient to alter the summation of nonsimultaneously activated synapses. The latency in Fig. 15*D* (1 nS) is nearly identical to that in *B*. Finally, in Fig. 15*F* (0.1 nS) the latency has become more complicated because of a nonmonotonic result when the stem becomes long and thin.

DISCUSSION

One aim of this study was to determine those morphological features of the macular afferent ending that need to be included in a compartmental model and those features that

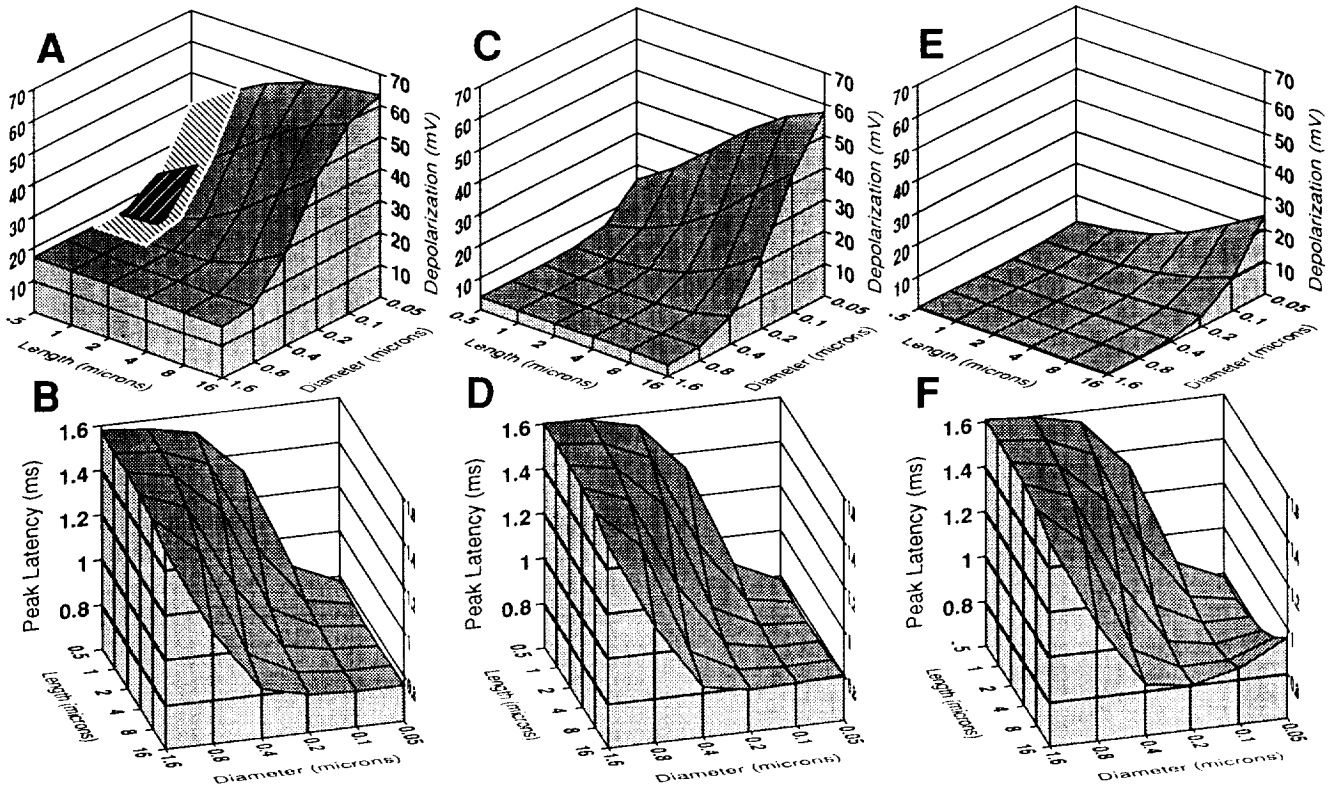

FIG. 15. Matrix of depolarization magnitude and latency as a function of stem length and diameter, and synaptic conductance. All parameters are as in Fig. 5. Recordings were made at the head of the process. *A* and *B*: synapse is located on the head of the process with g_{syn} = 5 nS. Large variations in voltage [46.2-mV increase (270%)] between the shortest, thickest and the longest, thinnest stems are produced in the simulations. Variations in latency are smaller [0.8-ms decrease (47%)]. *C* and *D*: g_{syn} = 1 nS. Depolarization varies with morphology more than in *A* [53.4-mV increase (1,340%)]. Latency is nearly identical to *B*. *E* and *F*: g_{syn} is further reduced to 0.1 nS. The variation in depolarization is reduced in absolute magnitude to 24.2 mV, but the percentage increase has expanded to 5,865% because of the extremely small depolarization of the shortest, thickest stems (0.4 mV). Latency has become more complicated because of a nonmonotonic result as the stem becomes long and thin.

can be collapsed to produce a simpler but equivalent structure for modeling. The criterion was whether a morphological parameter affected current flow and voltage sufficiently to alter the firing characteristics of the neuron or to influence the output from intrinsic efferent and recurrent synaptic connections. The results of this study demonstrate that certain details of macular morphology, which can be determined only with the aid of transmission electron microscopy (TEM), are essential to the model. Diameter, length, and location of spinelike processes influence the contribution of a synaptic input to AP generation and latency and affect the magnitude of depolarization near recurrent synapses. Therefore most of the morphological details observed with TEM cannot be collapsed when modeling the vestibular endorgan by compartmental methods. This is in contrast to conclusions reached for other neurons, which have more typical dendritic structures and a SIZ located proximal to a cell body (Durand et al. 1983; Jack and Redman 1971; Rall 1962, 1984; Rose and Vanner 1988). However, these morphological features do not affect the magnitude of depolarizations reaching the heads of efferent processes.

Selection of simulation parameter values

Values for synaptic conductance and membrane resistivity are not easily selected for compartmental simulations, because results suggested by in vitro and in vivo electrophysiological studies vary widely. We hoped to narrow the choices by examining the consequences of varying parameters across a range of reasonable values. Indirect methods of selecting the particular parameters are necessary because direct measurements of membrane resistivity and synaptic conductance are not available for vestibular primary afferents. One such indirect method is to use EPSP amplitude. EPSPs measured in primary afferents in the vestibular system of frogs (Rossi et al. 1977), lizards (Schessel et al. 1991), and toads (Sugai et al. 1991), and in the auditory system of goldfish (Furakawa et al. 1978), provide values between 0.5 and 1.0 mV. Although the morphology of afferents in these animals differs from that in mammals, our findings suggest that a 1.0 nS synaptic conductance is most appropriate for use in vestibular afferent simulations because 1.0 nS produces an appropriate-amplitude EPSP (see Fig. 9). Also, when 1.0 nS is used the number of simultaneously activated synapses necessary to produce an AP with minimal delay matches well with the number of synapses found within some rat type I hair cells, i.e., 6–10 synapses per cell. Altering membrane resistivity did not change the EPSP amplitude enough to provide a basis for choosing between the values tested. However, EPSP duration was closest to that obtained experimentally when the membrane resistivity was 5,000 Ωcm^2 (Fig. 8). Including an active SIZ in the simulation (Fig. 11) brought the EPSP duration even closer to measured values.

Effects of stem dimension

Our first simulations were conducted on morphologically realistic processes emanating from a short length of neuron branch. The difficulty in predicting the magnitude of depolarization for any particular real process led us to complete a systematic analysis of simplified processes with biologically appropriate stem lengths and diameters. This analysis clarified the relative contribution of stem length and diameter to depolarization magnitude. The results indicate that morphologically realistic dimensions are significant when modeling the final output of the afferent ending, i.e., an AP. Furthermore, using any single set of morphological measurements does not completely define the manner in which morphology affects the magnitude of depolarization or the latency. It is necessary to examine an appropriate range of stem lengths and diameters to appreciate the variation in voltage and latency (Chimento et al. 1991, 1992). Furthermore, the result of examining a range of membrane resistivities and synaptic conductances constrains the final selection of values for these variables.

Morphological details influence simulation results. For example, placing a process on a calyx rather than on a neuron branch resulted in a 7% decrease in depolarization (Fig. 7); simultaneously activated synapses did not sum linearly but lowered the magnitude of depolarization at the SIZ by 14% (Fig. 11); an afferent with four calyces contributed 40% less depolarization at the SIZ than an afferent with two calyces (compare Fig. 7, *A* and *D*). These purely morphological differences would be counterbalanced or further exaggerated by the choice of membrane electrical parameters.

If processes are viewed as electronic devices, the voltage drop across the stem of both afferent and efferent processes is controlled by impedance matching. There are two impedance matching problems: head to stem and stem to neuron branch. In afferent processes the head to stem impedance matching is a consequence of the ratio g_{syn}/g_{stem} (the conductance of the synapse divided by the conductance of the stem). The net effect of a synapse on depolarization of the neuron branch (or calyx) is determined by the ratio of the conductance loading provided by the neuron branch (or calyx) to the conductance of the stem. If g_{syn} is large and g_{stem} is small (i.e., the diameter of the stem is small), the process can act as a fixed voltage source (Koch et al. 1992), but only if the conductance of the neuron branch (or calyx) is small. On the other hand, if the conductance of the neuron branch is large compared with the stem, then the stem cannot transfer sufficient current to depolarize the neuron branch, i.e., there is an impedance mismatch. The consequence of this impedance mismatch is seen by comparing results of the long, thin stems in Fig. 5*A* with Fig. 15*A*. Under these conditions, impedance mismatch decreased the magnitude of depolarization by >60 mV (see also Shepherd and Brayton 1979, Fig. 2).

Efferent processes, because of their relatively small diameter, have a high input impedance compared with the neuron branch or calyx from which they emanate. Just as the high input impedance of an oscilloscope allows it to accurately reflect the voltage of some system, the high input impedance of stems of efferent processes allows the processes to accurately reflect the magnitude of depolarization within calyces and neuron branches. Thus efferent processes act as voltage followers. This result agrees with findings obtained in models of dendrites and dendritic spines by Shepherd and Brayton (1979).

Effects of process location

Our first insight from simulations of whole afferent endings was that process location affected net depolarization at the SIZ, but the significance of this effect could not be determined immediately. Of greater consequence was the overall size of the afferent, which greatly altered the magnitude of depolarization (Fig. 7). As the number of calyces and the length of neuron branches increased, the amplitude of the depolarization at the SIZ decreased. This is a function of the surface area of calyx membrane, which changes the charge-loading characteristics of the cell.

Baird et al. (1988) and Goldberg et al. (1990) assumed identical properties for synapses at all sites and a linear summation of inputs in their model. However, they found discrepancies between their experimental values and those predicted by their model. They then used compartmental models to calculate the expected synaptic voltages but were unable to improve the fit between actual and predicted synaptic gains. In contrast to the assumptions of Baird et al. (1988) and Goldberg et al. (1990), but in agreement with Rall (1967), Jack et al. (1983) and many others, the present results indicate that a single value cannot be applied to all synaptic inputs on all primary afferents. Also, synaptic inputs do not sum linearly (see below). Instead, it is necessary to determine the location of the synapses, the specific morphology of the processes, and the total morphology of the afferents to correctly specify the results of synaptic input.

Nonlinear summation of synaptic input

Another important insight regarding summation of synaptic inputs is the magnitude of its nonlinearity. In agreement with earlier work of Rall (1967) and of Jack et al. (1983), the present results demonstrate that the activation of multiple, dispersed synapses cannot be considered equal to the sum of many individual, idealized synapses. For network simulations, the nonlinear effects of placing synapses on the heads of processes with thin stems must be accounted for or the depolarization of the neuron will be overestimated.

The nonlinearity demonstrated in these simulations is even greater when a train of synaptic activation occurs. For example, the second, third, and further activations of the synaptic channels at the head of a process with a thin stem will not pass the same current allowed by the first activation. This is because the head of the process will remain depolarized. The electromotive driving force into the cell will be diminished until the local potential at the terminal head returns to resting. This result concurs with findings in dendritic spines of neostriatal spiny projection neurons (Wilson 1992).

Including active membrane

The addition of active (Hodgkin-Huxley) channels at the SIZ reduces the amplitude and duration of subthreshold depolarizations. Active channels serve to increase the temporal dynamics of the system by more rapidly returning the cell to resting potential. For a series of subthreshold responses, the contributions of individual synapses to depolarization of the afferent would be significantly less than estimated from simulations of passive neurons, especially if the synapses are not simultaneously activated. In contrast to most neuronal models that have the SIZ far removed from the sites of synaptic input, many of the terminal endings in the vestibular periphery are electrically close to the SIZ and all are in continuity with it. Continuity with the active membrane for spike generation requires inclusion of this active zone in simulations of synapses, even though the synapses may be located in a passive region of the cell.

Influences of distal spread of the AP

Vestibular afferent neurons are bipolar cells, structurally capable of bidirectional conductance of APs initiated along the axon. On histochemical grounds, the SIZ of nerve fibers with long unmyelinated neuron branches is likely located at the first heminode (Ross et al. 1991; Saidel 1988). There is no cell body separating the SIZ from the terminal endings. Therefore the typical cellular conditions that might produce attenuation of the depolarizing effects of an AP on the most distal calyx processes are not present. Dendrites on classical neurons in the CNS tend to be much longer and more branched than macular endings, electrically isolating the distal tips of the dendrite from the SIZ.

The primary purpose of the AP is to transmit depolarization rapidly along the axon toward the CNS. A secondary consequence of the AP is a large, rapid, synchronous spread of depolarization distally into the primary afferent ending. With minimal delay, all the calyces on an afferent that has fired will be isopotential. Likewise, all the neuron branches, process stems, and process heads will be nearly isopotential. Simultaneous with the AP, sufficient depolarization to release transmitter from the efferent endings will arrive at the efferent heads (i.e., >20 mV depolarization).

Moreover, as the distal spread of depolarization approaches 0 mV, synaptic input to the afferent will be altered, thereby changing the discharge characteristics of the nerve fiber. When the depolarization at the head exceeds the reversal potential of the synaptic channels (0 mV), the electromotive driving force at the synapse will change from inward to outward, shunting current out of the cell. Therefore, when the cell is depolarized by the distal spread of the AP, the inward synaptic current will first slow and then reverse when the local potential is >0 mV. In some afferents, no inward flow of ions will pass through the synapse beginning 0.3 ms after AP onset, and this effect will last for nearly 0.4 ms (Fig. 14). Any postsynaptic channels that open will provide the afferent ending with a more rapid return to resting, not further depolarization. Therefore during an AP the electromotive driving force acting at a synapse would modulate the flow of current through the synaptic channel, acting as an "excitatory self inhibition." This modulation could have consequences for the rate and regularity of repetitive firing of the primary afferent.

The distal spread of the AP could also act as a source of depolarization for long-term potentiation (LTP) (Brown et al. 1990; Collingridge and Bliss 1987; Collingridge et al. 1983; Cotman and Monagham 1988; Lynch et al. 1983). This depolarization will occur with nearly equal magnitude and latency at all processes of a specific afferent (Figs. 11 and 12). The timing and magnitude of the depolarization would be sufficient to produce LTP and would occur only with AP firing.

Possible roles of efferent processes

Our results indicate that all efferent processes emanating from a single primary afferent, regardless of process morphology, receive synchronous depolarization sufficient to provide a unified output to adjacent cells in the macula. The consequences of activating the efferent processes depend on whether they form excitatory or inhibitory synapses. The neurotransmitter at these efferent processes is currently unknown.

A common inhibitory neurotransmitter in the CNS is γ-aminobutyric acid (GABA). GABA has been localized to the vestibular endorgan in hair cells and primary afferents (Didier et al. 1990; Usami et al. 1987a,b, 1989; Ylikoski et al. 1989) but is differentially localized according to the species examined. Nonmammalian species contain GABAergic elements within the hair cells, whereas mammals tend to contain GABA in afferent fibers (guinea pig) or efferent fibers (squirrel monkey). In the rat, only the upper parts of the calyces in the sensory epithelia showed evidence of GABA (Ylikoski et al. 1989).

The presence of GABA suggests that some synapses in the macula are inhibitory. A large percentage of the processes intrinsic to the macula are vesiculated and presynaptic to adjacent type II hair cells and other primary afferents (Ross et al. 1986). A possible function for the unusual arrangement of these endings is lateral inhibition, such as the center/surround organization in the retina. However, if these peripheral endings are GABAergic and the central terminations of the afferents in the vestibular nucleus are excitatory (as they most likely are), we are left with a single neuron producing two different neurotransmitters with opposite actions. The colocalization of the excitatory and inhibitory neurotransmitters glutamate and GABA, although uncommon, has been found in hippocampal mossy fibers (Sandler and Smith 1991).

Another interpretation is based on the ultrastructural morphology of the efferent synapses on type II hair cells. The morphology of the synapses at efferent terminals fits the morphology of c synapses: large presynaptic boutons containing spherical vesicles; a long, narrow synaptic cleft; and a large subsynaptic cistern (Conradi 1969; McLaughlin 1972; Pullen 1988). C synapses at other sites have been shown to be cholinergic and therefore excitatory (Connaughton et al. 1986). However, although the synapses are initially excitatory, in some cases they produce a long-duration postsynaptic hyperpolarization due to release of calcium from the subsynaptic cistern. The increased internal concentration of Ca^{2+} opens calcium-activated potassium channels (Fujimoto et al. 1980).

A further function of cholinergic processes synapsing on adjacent type II hair cells could be to activate contractile mechanisms within the cells (Ashmore and Holley 1988; Brownell et al. 1985; Slepecky 1989). A change in the linkage between the otoconial "test mass" and the sensory cells could alter the dynamics of the system.

Conclusions

The major questions posed in this study were whether small details of morphology, such as the size and location of neuronal processes, could influence the output of a vestibular afferent, and whether a knowledge of morphological details could guide the selection of values for simulation parameters. The conclusion that arises from our simulations is that the magnitude of depolarization for any particular afferent process depends on a combination of stem length and diameter. Furthermore, including these details provides constraints that aid in selecting membrane and synapse parameter values. When the small effects produced by these and other individual pieces of an entire afferent terminal are combined, the final output of an afferent will be altered. For example, a change in the number of activated synapses can produce major alterations in AP latency and changing membrane resistivity can alter the number of synapses necessary to reach AP threshold (Fig. 12).

These results demonstrate that the measurements available only from TEM are necessary for accurate biological simulations. Determining which morphological details are biologically significant requires simulation of the whole vestibular afferent terminal, including active and passive membrane.

We thank J. Varelas and L. Cutler for assistance with electron microscopy. We also thank D. Perkel, L. Stone, M. Sutter, and L. Waldman for review of an earlier draft of the manuscript.

This research was supported by a National Academy of Sciences, National Research Council Research Associateship to T. C. Chimento, the National Aeronautics and Space Administration and National Institute of Mental Health Grant MH-47305-01 to M. D. Ross.

Address reprint requests to T. C. Chimento.

Received 3 May 1993; accepted in final form 19 January 1994.

REFERENCES

ASHMORE, J. F. AND HOLLEY, M. C. Temperature dependence of a fast motile response in isolated outer hair cells of the guinea-pig cochlea. *Q. J. Exp. Physiol.* 73: 143–145, 1988.

BAIRD, R. A., DESMADRYL, G., FERNANDEZ, C., AND GOLDBERG, J. M. The vestibular nerve of the chinchilla. II. Relation between afferent response properties and peripheral innervation patterns in the semicircular canals. *J. Neurophysiol.* 60: 182–203, 1988.

BROWN, T. H., KAIRISS, E. W., AND KEENAN, C. L. Hebbian synapses: biophysical mechanisms and algorithms. *Annu. Rev. Neurosci.* 13: 475–511, 1990.

BROWN, T. H., PERKEL, D. H., NORRIS, J. C., AND PEACOCK, J. H. Electrotonic structure and specific membrane properties of mouse dorsal root ganglion neurons. *J. Neurophysiol.* 45: 1–15, 1981.

BROWNELL, W. E., BADER, C. R., BERTRAND, D., AND RIBAUPIERRE, Y. Evoked mechanical responses of isolated cochlear outer hair cells. *Science Wash. DC* 227: 194–196, 1985.

CHERUBINI, E., NORTH, R. A., AND WILLIAMS, J. T. Synaptic potentials in rat locus coeruleus neurons. *J. Physiol. Lond.* 406: 431–442, 1988.

CHIMENTO, T. C., DOSHAY, D. G., AND ROSS, M. D. *Compartmental Models of Current Flow in Rat Macular Calyceal and Nerve Branch Processes Using 3-Dimensional Reconstructions From Electron Micrographs of Serial Sections.* Society for Neuroscience, 21st Annual Meeting, New Orleans, LA, 1991.

CHIMENTO, T. C., DOSHAY, D. G., AND ROSS, M. D. Compartmental modeling of macular primary neuron branch processes. In: *Neural Systems, Analysis and Modeling.* edited by F. H. Eeckman. Norwell, MA: Kluwer, 1992, vol. 2, p. 355–363.

COLEMAN, P. A. AND MILLER, R. F. Measurement of passive membrane parameters with whole-cell recording from neurons in the intact amphibian retina. *J. Neurophysiol.* 61: 218–230, 1989.

COLLINGRIDGE, G. L. AND BLISS, T. V. P. NMDA receptors—their role in long-term potentiation. *Trends Neurosci.* 10: 288–293, 1987.

COLLINGRIDGE, G. L., KEHL, S. L., AND MCLENNAN, H. Excitatory amino acids in synaptic transmission in the Schaffer collateral—commissural pathway of the rat hippocampus. *J. Physiol. Lond.* 334: 33–46, 1983.

CONNAUGHTON, M., PRIESTLEY, J. V., SOFRONIEW, M. V., ECKENSTEIN,

F., AND CUELLO, A. C. Inputs to motoneurons in the hypoglossal nucleus of the rat: light and electron microscopic immunocytochemistry for choline acetyltransferase, substance P and enkephalins using monoclonal antibodies. *Neuroscience* 17: 205–224, 1986.

CONRADI, S. Ultrastructure and distribution of neuronal and glial elements on the motoneuron surface in the lumbosacral spinal cord of the adult cat. *Acta. Physiol. Scand. Suppl.* 332: 5–48, 1969.

COTMAN, C. W. AND MONAGHAN, D. T. Excitatory amino acid neurotransmission: NMDA receptors and Hebb-type synaptic plasticity. *Annu. Rev. Neurosci.* 11: 61–80, 1988.

DIDIER, A., DUPONT, J., AND CAZALS, Y. GABA immunoreactivity of calyceal nerve endings in the vestibular system of the guinea pig. *Cell Tissue Res.* 260: 415–419, 1990.

DURAND, D., CARLEN, P. L., GUREVICH, N., HO, A., AND KUNOV, H. Electrotonic parameters of rat dentate granule cells measured using short current pulses and HRP staining. *J. Neurophysiol.* 50: 1080–1097, 1983.

FUJIMOTO, S., YAMAMOTO, K., KUBA, K., MORITA, K., AND KATO, E. Calcium localization in the sympathetic ganglion of the bullfrog and effects of caffeine. *Brain Res.* 202: 21–32, 1980.

FURUKAWA, T., HAYASHIDA, Y., MATSUURA, S. Quantal analysis of the size of excitatory post-synaptic potentials at synapses between hair cells and afferent nerve fibres in goldfish. *J. Physiol. Lond.* 276: 211–226, 1978.

GOLDBERG, J. M., LYSAKOWSKI, A., AND FERNANDEZ, C. Morphophysiological and ultrastructural studies in the mammalian cristae ampullares. *Hear. Res.* 49: 89–102, 1990.

HARRIS, D. AND STEVENS, J. K. Dendritic spines of CA 1 pyramidal cells in the rat hippocampus: serial electron microscopy with reference to their biophysical characteristics. *J. Neurosci.* 9: 2982–2997, 1989.

HESTRIN, S., NICOLL, R. A., PERKEL, D. J., AND SAH, P. Analysis of excitatory synaptic action in pyramidal cells using whole-cell recording from rat hippocampal slices. *J. Physiol. Lond.* 422: 203–225, 1990.

HINES, M. A program for simulation of nerve equations with branching geometries. *Int. J. Biomed. Comput.* 24: 55–68, 1989.

HINES, M. *Neuron and Hoc Interpreter.* Durham, NC: Duke Univ. Medical Center, 1991.

JACK, J. J. B., NOBLE, D., AND TSIEN, R. W. *Electric Current Flow in Excitable Cells.* Oxford, UK: Clarendon, 1983.

JACK, J. J. B. AND REDMAN, S. J. An electrical description of the motoneuron and its application to the analysis of synaptic potentials. *J. Physiol. Lond.* 215: 321–352, 1971.

JOHNSTON, D. AND BROWN, T. H. Interpretation of voltage-clamp measurements in hippocampal neurons. *J. Neurophysiol.* 50: 464–483, 1983.

KINNAMON, J. C., YOUNG, S. J., SHERMAN, T. J. *IBM PC-based Three-Dimensional Reconstruction Program. Laboratory for High Voltage Electron Microscopy.* Boulder, CO: Univ. of Colorado, 1986.

KOCH, C., ZADOR, A., AND BROWN, T. H. Dendritic spines: convergence of theory and experiment. *Science Wash. DC* 256: 973–974, 1992.

LYNCH, G., LARSON, J., KELSO, S., BARRIONEUVO, G., AND SCHOTTLER, F. Intracellular injections of EGTA block induction of hippocampal long term potentiation. *Nature Lond.* 305: 719–721, 1983.

MCLAUGHLIN, B. J. The fine structure of neurons and synapses in the motor nuclei of the cat spinal cord. *J. Comp. Neurol.* 144: 429–460, 1972.

PULLEN, A. H. Feline C-type terminals possess synaptic sites associated with a hypolemmal cistern and Nissl body. *Neurosci. Lett.* 84: 143–148, 1988.

RAJAN, R. AND JAHNSTONE, B. M. Biaural acoustic stimulation exercises protective effects at the cochlea that mimic the effects of electrical stimulation of an auditory efferent pathway. *Brain Res.* 459: 241–255, 1988.

RALL, W. Theory of physiological properties of dendrites. *Ann. NY Acad. Sci.* 96: 1071–1092, 1962.

RALL, W. Distinguishing theoretical synaptic potentials computed for different soma-dendritic distributions of synaptic input. *J. Neurophysiol.* 30: 1138–1168, 1967.

RALL, W. Time constants and electrotonic length of membrane cylinders and neurons. *Biophys. J.* 9: 1483–1508, 1969a.

RALL, W. Distributions of potential in cylindrical coordinates and time constants for a membrane cylinder. *Biophys. J.* 9: 1509–1541, 1969b.

RALL, W. Dendritic neuron theory and dendrodendritic synapses in a simple cortical system. *Handbook of Physiology. The Nervous System. Cellular Biology of Neurons.* Bethesda, MD: Am. Physiol. Soc., 1984, sect. 1, vol. III, p. 552–565.

RALL, W. AND SHEPHERD, G. M. Theoretical reconstruction of field potentials and dendrodendritic synaptic interactions in olfactory bulb. *J. Neurophysiol.* 31: 884–915, 1968.

RANDALL, A. D., SCHOFIELD, J. G., AND COLLINGRIDGE, G. L. Whole cell patch clamp recordings of an NMDA receptor mediated synaptic current in rat hippocampal slices. *Neurosci. Lett.* 114: 191–196, 1990.

ROSE, P. K. AND VANNER, S. J. Differences in somatic and dendritic specific membrane resistivity of spinal motoneurons: an electrophysiological study of neck and shoulder motoneurons in the cat. *J. Neurophysiol.* 60: 149–165, 1988.

ROSS, M. D., CUTLER, L., DOSHAY, D., CHENG, R., AND NADDAF, A. A new theory of macular organization based on computer-assisted 3-D reconstruction, Monte Carlo simulation and symbolic modeling of vestibular maculas. *Acta Otolaryngol. Suppl.* 481: 11–14, 1991.

ROSS, M. D., CUTLER, L., MEYER, G., LAM, T., AND VAZIRI, P. 3-D components of a biological neural network visualized in computer generated imagery. I. Macular receptive field organization. *Acta Otolaryngol.* 109: 83–92, 1990a.

ROSS, M. D., MEYER, G., LAM, T., CUTLER, L., AND VAZIRI, P. 3-D components of a biological neural network visualized in computer generated imagery. II. Macular neural network organization. *Acta Otolaryngol.* 109: 235–244, 1990b.

ROSS, M. D., ROGERS, C. M., AND DONOVAN, K. M. Innervation patterns in rat saccular macula: a structural basis for complex sensory processing. *Acta Otolarygol.* 102: 75–86, 1986.

ROSSI, M. L., VALLI, P., AND CASELLA, C. Post-synaptic potentials recorded from afferent nerve fibres of the posterior semicircular canal in the frog. *Brain Res.* 135: 67–75, 1977.

SAIDEL, W. M. Variations of trigger zones in vestibular afferent fibers of fish. *Neurosci. Lett.* 84: 161–166, 1988.

SANDLER, R. AND SMITH, A. D. Coexistence of GABA and glutamate in mossy fiber terminals of the primate hippocampus: an ultrastructural study. *J. Comp. Neurol.* 303: 177–192, 1991.

SCHESSEL, D. A., GINZBERG, R., AND HIGHSTEIN, S. M. Morphophysiology of synaptic transmission between type I hair cells and vestibular primary afferents. An intracellular study employing horseradish peroxidase in the lizard, *Calotes versicolor. Brain Res.* 544: 1–16, 1991.

SEGEV, I. AND RALL, W. Computational study of an excitable dendritic spine. *J. Neurophysiol.* 60: 499–522, 1988.

SHEPHERD, G. M. AND BRAYTON, R. K. Computer simulation of a dendrodendritic synaptic circuit for self- and lateral-inhibition in the olfactory bulb. *Brain Res.* 175: 377–382, 1979.

SHEPHERD, G. M., BRAYTON, R. K., MILLER, J. P., SEGEV, I., RINZEL, J., AND RALL, W. Signal enhancement in distal cortical dendrites by means of interactions between active dendritic spines. *Proc. Natl. Acad. Sci. USA* 82: 2192–2195, 1985.

SLEPECKY, N. Cytoplasmic actin and cochlear outer hair cell motility. *Cell Tissue Res.* 257: 69–75, 1989.

SUGAI, T., SUGITANI, M., AND OOYAMA, H. Effects of activation of the divergent efferent fibers on the spontaneous activity of vestibular afferent fibers in the toad. *Jpn. J. Physiol.* 41: 217–232, 1991.

USAMI, S.-I., HOZAWA, J., TAZAWA, M., IGARASHI, M., THOMPSON, G., WU, J.-Y., AND WENTHOLD, R. J. Immunocytochemical study of the GABA system in chicken vestibular endorgans and the vestibular ganglion. *Brain Res.* 503: 214–218, 1989.

USAMI, S.-I., IGARASHI, M., AND THOMPSON, G. C. GABA-like immunoreactivity in the squirrel monkey vestibular endorgans. *Brain Res.* 417: 367–370, 1987a.

USAMI, S.-I., IGARASHI, M., AND THOMPSON, G. C. GABA-like immunoreactivity in the chick vestibular end organs. *Brain Res.* 418: 383–387, 1987b.

WILSON, C. Nonlinear synaptic integration in neostriatal spiny neurons. In: *Neural Systems, Analysis and Modeling.* edited by F. H. Eeckman. Norwell, MA: Kluwer, 1992, vol. 2, p. 393–405.

YAMAGUCHI, K. AND OHMORI, H. Voltage-gated and chemically gated ionic channels in the cultured cochlear ganglion neurone of the chick. *J. Physiol. Lond.* 420: 185–206, 1990.

YLIKOSKI, J., PIRVOLA, U., HAPPOLA, O., PANULA, P., AND VIRTANEN, I. Immunohistochemical demonstration of neuroactive substances in the inner ear of rat and guinea pig. *Acta Otolaryngol.* 107: 417–423, 1989.

YOUNG, S. J., ROYER, S. M., GROVES, P. M., AND KINNAMON, J. C. Three-dimensional reconstructions from serial micrographs using the IBM PC. *J. Electron Microsc. Tech.* 6: 207–217, 1987.